Spin-Orbit Interaction in Graphite

G. DRESSELHAUS AND M. S. DRESSELHAUS
Lincoln Laboratory, Massachusetts Institute of Technology, Lexington, Massachusetts*
(Received 3 May 1965)

Using symmetry arguments, the effective-mass Hamiltonian including spin-orbit interaction is derived for energy bands with extrema near the vertical edge of the hexagonal prism which represents the Brillouin zone of graphite. The energy bands in the plane normal to the vertical edge are described by $\mathbf{k}\cdot\mathbf{p}$ perturbation theory, whereas along the edge a Fourier expansion is used for all the matrix elements. It is shown that spin-orbit interaction lifts all band degeneracies (other than the Kramers degeneracy), and affects the graphite Fermi-surface topology at the Brillouin-zone boundary $k_z=\pm\pi/c_0$, where two de Haas–van Alphen periods are predicted. Magnetic energy levels for a static magnetic field $\mathbf{H}\|\mathbf{c}$ are obtained by solution of the effective-mass Hamiltonian. Selection rules for infrared interband transitions are discussed. An evaluation of the spin-orbit band parameters is suggested by analysis of structure in the low-quantum-limit magnetoreflection data and of the low-frequency de Haas–van Alphen oscillations.

I. INTRODUCTION

THE Slonczewski-Weiss (S-W) band model[1] has been frequently used to interpret experiments relating to the electronic band structure of graphite.[2] In the past this model has been very successful in explaining many of these experimental results. Recently, the magnetoreflection and low-frequency de Haas–van Alphen measurements have become so precise, that a more refined theory is now needed to explain certain small departures from the usual S-W band model. Although the spin-orbit interaction is small, it has an important effect on the energy bands in the neighborhood of band degeneracies. Since the Fermi surface always lies near a band degeneracy, this interaction is responsible for measurable deviations from the usual S-W band model in the vicinity of certain critical points along the vertical edges of the Brillouin zone. In the case of the magnetoreflection experiment, a nonzero band gap is found for interband transitions associated with point K in the Brillouin zone, indicating a spin-orbit splitting of the doubly degenerate E_3 bands. Furthermore, considerable structure is observed in the magnetoreflection experiment in the limit of low photon energy and high magnetic fields, suggestive of a spin splitting of the resonance lines.[3] A detailed analysis of the low-frequency de Haas–van Alphen oscillation associated with the Fermi surface about point H in the Brillouin zone gives evidence for a spin-orbit splitting of the π bands in the vicinity of the Brillouin-zone corner.[4,5]

The effect of the spin-orbit interaction was previously considered by Slonczewski[6] in his derivation of the effective-mass Hamiltonian. By use of tight-binding arguments, he concluded that this effect was small compared with other interactions, and therefore no detailed calculation of the spin-orbit interaction was given at that time.[1] More recently, McClure and Yafet[7] used spin-orbit interaction to calculate the small g shift observed in the spin-resonance experiments of Wagoner.[8] Since the measured g shift arises from averaging the contribution of all electron and hole transitions about the Fermi surface, certain simplifications were made in order to obtain numerical results. These simplifications amounted to introducing a minimum number of spin-orbit band parameters. Tight-binding arguments were employed to show which spin-orbit terms were large and these were all set equal to one another, while the smaller terms were ignored. Thus, with only one spin-orbit band parameter, McClure and Yafet were able to obtain good agreement with experiment for the temperature dependence of the g shift, although a larger value for one of the other band parameters was required ($\Delta\sim 0.1$ eV) than is indicated by other experiments.[5,9]

Since more refined experiments relevant to the spin-orbit interaction in graphite are now available, a more detailed theory of the effect has been developed. The point of view adopted in this paper differs somewhat from previous work in that symmetry considerations are emphasized more strongly. Tight-binding arguments can then be used to obtain a physical interpretation of the various spin-orbit band parameters which are required by symmetry. The numerical evaluation of these parameters can, in principle, be made from suitable experimental measurements. Since the effective mass Hamiltonian is constructed by symmetry arguments

* Operated with support from the U. S. Air Force.

[1] J. C. Slonczewski and P. R. Weiss, Phys. Rev. **109**, 272 (1958).

[2] R. R. Haering and S. Mrozowski, *Progress in Semiconductors* (John Wiley & Sons, Inc., New York, 1960), Vol. 5, p. 273. J. W. McClure, IBM J. Res. Develop. **8**, 255 (1964). The first of these review articles contains an extensive bibliography on all work on graphite prior to 1960.

[3] M. S. Dresselhaus and J. G. Mavroides, Carbon **1**, 263 (1963).

[4] D. E. Soule, IBM J. Res. Develop. **8**, 268 (1964).

[5] S. J. Williamson, S. Foner, and M. S. Dresselhaus, Proceedings of the Ninth International Conference on Low Temperature Physics, Columbus, Ohio, 1964 (to be published); Bull. Am. Phys. Soc. **10**, 109 (1965).

[6] J. C. Slonczewski, thesis, Rutgers University, 1955 (unpublished).

[7] J. W. McClure and Y. Yafet, *Proceedings of the Fifth Conference on Carbon* (Pergamon Press, Inc., Oxford and New York, 1960), p. 22.

[8] G. Wagoner, Phys. Rev. **118**, 647 (1960).

[9] J. G. Mavroides and M. S. Dresselhaus, Bull. Am. Phys. Soc. **10**, 109 (1965).

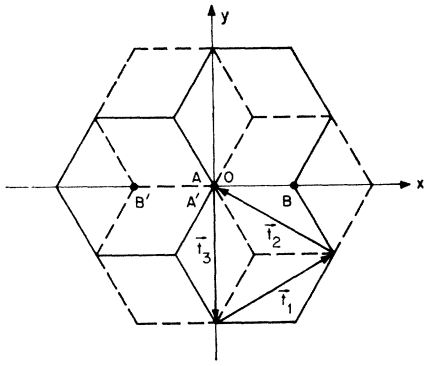

FIG. 1. Projection of the graphite lattice on a layer plane. The atoms A and B lie in the plane, while the A' and B' atoms lie in another plane displaced along the plane normal by $\mathbf{t}_4/2$. The basis vectors for the primitive cell containing atomic sites A, A', B, and B' are $\mathbf{t}_1$, $\mathbf{t}_2$, and $\mathbf{t}_4$.

alone, the derivation given here applies equally well to all other materials having the same crystal symmetry. Similar Hamiltonians could be derived for the analysis of the electronic band structure of other semimetals with different crystal symmetry.

In Sec. II, the derivation of the effective-mass Hamiltonian is given. Both the $\mathbf{k}\cdot\mathbf{p}$ perturbation terms and the spin-orbit terms are treated on equal footing. Symmetry considerations are used to establish the form of the Hamiltonian in the vicinity of a symmetry axis (in this case the Brillouin-zone edge). The dependence of the matrix elements of the Hamiltonian on the wave vector k_z along the symmetry axis is found explicitly, still using symmetry arguments.

In Sec. III, the effect of the spin-orbit interaction on the Fermi surface is discussed. In particular, without spin-orbit effects, neither the degenerate Fermi-surface cross section nor the effective mass at the Brillouin-zone boundary is extremal. By including spin-orbit interaction, certain band degeneracies near the zone corner are lifted, thus resulting in two extremal Fermi-surface cross sections and associated effective masses at the Brillouin-zone boundary, $k_z=\pm\pi/c_0$. These extremal areas are related to the low-frequency de Haas–van Alphen oscillation.

The effect of the spin-orbit interaction on the energy bands in a magnetic field is considered in Sec. IV. A specific application of these magnetic energy levels is made to obtain selection rules for interband transitions in the magnetoreflection experiment. Finally, the experimental determination of the various band parameters introduced in the effective-mass Hamiltonian is discussed.

II. HAMILTONIAN FOR π BANDS IN GRAPHITE

The form of the effective-mass Hamiltonian for the π bands in graphite follows directly from the symmetry of the lattice,[2] which is illustrated in Fig. 1. The primitive unit cell contains four atoms labeled A, A', B, and B'. The A and B atoms are in the same layer plane, whereas the atoms A' and B' are on a layer plane displaced by $\mathbf{t}_4/2$. The origin of the unit cell is taken at an A site, so that the position vectors of the atoms in the unit cell are given by

$$\mathbf{t}_A=0, \qquad \mathbf{t}_{A'}=\mathbf{t}_4/2,$$
$$\mathbf{t}_B=(\mathbf{t}_1-\mathbf{t}_2)/3, \quad \mathbf{t}_{B'}=-(\mathbf{t}_1-\mathbf{t}_2)/3+\mathbf{t}_4/2, \tag{1}$$

in which the $\mathbf{t}_1$, $\mathbf{t}_2$, and $\mathbf{t}_4$ are primitive translation vectors for a simple hexagonal Bravais lattice, with

$$|\mathbf{t}_i|=a_0=2.46\ \text{Å}, \quad i=1, 2, 3$$
$$|\mathbf{t}_4|=c_0=6.74\ \text{Å}, \tag{2}$$

the numerical values for graphite at room temperature.[2] The reciprocal lattice vectors derived from the primitive translation vectors are denoted by $\mathbf{K}_i$, in which

$$\mathbf{K}_i\cdot\mathbf{t}_j=2\pi\delta_{ij}; \quad i, j=1, 2, 4 \tag{3}$$

and the half-vectors $\mathbf{K}_i/2$ are indicated in Fig. 2, showing the first Brillouin zone which these vectors define. The graphite Fermi surface lies near the six zone edges labeled HKH and $H'K'H'$. The wave vector to one of these edges, designated in Fig. 2 by $\mathbf{k}_s$, is given by

$$\mathbf{k}_s=\tfrac{2}{3}\mathbf{K}_1-\tfrac{1}{3}\mathbf{K}_2+k_z\hat{e}_z, \tag{4}$$

in which $\hat{e}_z$ is a unit vector along the $\mathbf{K}_4$ axis, and all the edges are equivalent.

The character table for the double group of the wave vector $\mathbf{k}_s$, denoted by $G(S)$, is given in Table I. The symmetry operations on the wave vector include rotations by $\pm 2\pi/3$ and glide reflections in the $(t_4 t_i)$ planes. In this table, the representations S_1, S_2, and S_3 give the transformation properties of the spatial part of the wave functions, whereas the spin functions transform as $D_{1/2}$.[10] Thus, the total wave functions (space times spin) transform as the direct products, $(S_i\times D_{1/2})$, $i=1, 2, 3$. The decomposition of the direct products $(S_i\times D_{1/2})$ are included in Table I. This decomposition immediately

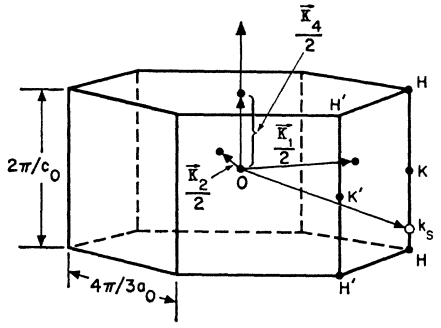

FIG. 2. First Brillouin zone for graphite. The basis vectors of the reciprocal lattice $\mathbf{K}_1$, $\mathbf{K}_2$, and $\mathbf{K}_4$ are indicated. The vector $\mathbf{k}_s$ to a general point along the zone edge is also shown.

[10] R. J. Elliott, Phys. Rev. **96**, 280 (1954).

TABLE I. The double group $G(S)$ and its small representations. Here $\alpha=\exp(-i\mathbf{k}_s\cdot\mathbf{t}_4/2)$, S_4 and S_5 are degenerate by time reversal, $D_{1/2}$ is the two-dimensional representation for the transformation of the spin-wave functions, and

$$S_1\times D_{1/2}=S_6,$$
$$S_2\times D_{1/2}=S_6,$$
$$S_3\times D_{1/2}=S_4+S_5+S_6,$$

are direct products.

Operator	Definition
ϵ	identity
δ_3, δ_3^{-1}	rotations by $\pm 2\pi/3$ about z axis
ρ_1, ρ_2, ρ_3	reflection in $(t_4 t_i)$ planes, $i=1, 2, 3$
$\mathcal{O}^*$	symmetry operation $\mathcal{O}$ followed by rotation of 2π

	Representations					
Group elements	S_1	S_2	S_3	S_4	S_5	S_6
$(\epsilon\|0)$	1	1	2	1	1	2
$(\delta_3\|0)$, $(\delta_3^{-1}\|0)$	1	1	-1	-1	-1	1
$(\rho_i\|\frac{1}{2}\mathbf{t}_4)$	α	$-\alpha$	0	$i\alpha$	$-i\alpha$	0
$(\epsilon\|0)^*$	1	1	2	-1	-1	-2
$(\delta_3\|0)^*$, $(\delta_3^{-1}\|0)^*$	1	1	-1	1	1	-1
$(\rho_i\|\frac{1}{2}\mathbf{t}_4)^*$	α	$-\alpha$	0	$-i\alpha$	$i\alpha$	0

shows that by including the effect of the electron spin through the spin-orbit interaction, the S_3 spatial degeneracy is lifted. Since the representations S_4 and S_5 are degenerate by time-reversal symmetry, all energy levels along the zone edge are doubly degenerate. In the remainder of this section, the symmetry considerations given above are applied to obtain an explicit form for the effective-mass Hamiltonian of graphite.

The one-electron Hamiltonian for a periodic potential $V(\mathbf{r})$ including spin-orbit interaction is

$$\mathcal{H}=(p^2/2m)+V(\mathbf{r})+(\hbar/4m^2c^2)(\nabla V\times\mathbf{p})\cdot\boldsymbol{\sigma}, \quad (5)$$

in which the spin-orbit interaction is given by the last term,

$$\mathcal{H}_{s.o.}=\mathbf{L}\cdot\boldsymbol{\sigma}, \quad (6)$$

and the operator $\mathbf{L}$ defined by

$$\mathbf{L}=(\hbar/4m^2c^2)(\nabla V\times\mathbf{p}) \quad (7)$$

transforms as the angular momentum. "$\mathbf{k}\cdot\mathbf{p}$" perturbation theory is used to obtain the energy levels at a general point in the vicinity of the Brillouin-zone edge, $\mathbf{k}=\mathbf{k}_s+\boldsymbol{\kappa}$. The perturbation obtained from Eq. (5) is then

$$\mathcal{H}'=(\hbar/m)\boldsymbol{\kappa}\cdot[\mathbf{p}+(1/4mc^2)\boldsymbol{\sigma}\times(\nabla V)]+\hbar^2\kappa^2/2m. \quad (8)$$

Since the Hamiltonian in Eq. (5) is assumed to be solved for all points $\mathbf{k}_s$, the wave vector $\boldsymbol{\kappa}$ in the perturbation can be taken in a $\mathbf{K}_1\mathbf{K}_2$ layer plane. The quadratic term $(\hbar^2\kappa^2/2m)$ is a c number and contributes only to the diagonal matrix elements of the Hamiltonian. The term in Eq. (8) derived from the spin-orbit interaction could, in principle, be treated within the framework of this calculation. Since this term is expected to be much smaller than the spin-orbit interaction term in Eq. (6) and, also, since this term gives rise to no additional band splittings, it is neglected in the explicit calculation, presented here.

It is convenient to write the spin-orbit and "$\mathbf{k}\cdot\mathbf{p}$" perturbation Hamiltonians in terms of the raising and lowering operators: $p_\pm=p_x\pm ip_y$, $L_\pm=L_x\pm iL_y$,

$$\mathcal{H}_{s.o.}=L_z\sigma_z+\tfrac{1}{2}(L_+\sigma_-+L_-\sigma_+), \quad (9)$$

and

$$\mathcal{H}'=(\hbar/2m)(\kappa_+p_-+\kappa_-p_+). \quad (10)$$

Since both the linear- and angular-momentum operators are unaffected by translations, their transformation properties under the glide operations $(\rho_i|\mathbf{t}_4/2)$ are obtained from those for the wave functions given in Table I by setting $\mathbf{k}_s=0$ or $\alpha=1$. These irreducible representations are defined as $\Gamma_i\equiv S_i(\mathbf{k}_s=0)$ and pertain to a point group derived from $G(S)$. The linear and angular momentum components p_z and L_z transform as the irreducible representation Γ_1 and Γ_2, respectively, while $p_\pm$ and $L_\pm$ transform as Γ_3.

The matrix elements of the Hamiltonian are taken between wave functions which transform as the irreducible representations S_1, S_2, and S_3 and are denoted by Ψ_{11}, Ψ_{21}, Ψ_{31}, and Ψ_{32}, respectively, following the notation of Slonczewski and Weiss.[1] These wave functions are constructed by taking appropriate linear combinations of the p_z wave functions (π functions) on the A, A', B, B' lattice sites. An explicit matrix representation of the two dimensional S_3 representation is

$$(\epsilon|\mathbf{0})=\begin{pmatrix}1&0\\0&1\end{pmatrix},\qquad (\delta_3|\mathbf{0})=\begin{pmatrix}\omega^{-1}&0\\0&\omega\end{pmatrix},$$
$$(\delta_3^{-1}|\mathbf{0})=\begin{pmatrix}\omega&0\\0&\omega^{-1}\end{pmatrix},\quad (\rho_1|\tfrac{1}{2}\mathbf{t}_4)=\alpha\begin{pmatrix}0&1\\1&0\end{pmatrix}, \quad (11)$$
$$(\rho_2|\tfrac{1}{2}\mathbf{t}_4)=\alpha\begin{pmatrix}0&\omega^{-1}\\\omega&0\end{pmatrix},\quad (\rho_3|\tfrac{1}{2}\mathbf{t}_4)=\alpha\begin{pmatrix}0&\omega\\\omega^{-1}&0\end{pmatrix},$$

in which

$$\omega=\exp\{2\pi i/3\},$$

and

$$\alpha=\exp\{-i\mathbf{k}_s\cdot\mathbf{t}_4/2\}.$$

The diagonal matrix elements of the Hamiltonian, taken in the representation which transforms as the irreducible representations of the group of the wave vector $\mathbf{k}_s$, are denoted by

$$E_1(k_z)=(\Psi_{11}|\mathcal{H}_0|\Psi_{11}),$$
$$E_2(k_z)=(\Psi_{21}|\mathcal{H}_0|\Psi_{21}), \quad (12)$$
$$E_3(k_z)=(\Psi_{31}|\mathcal{H}_0|\Psi_{31})=(\Psi_{32}|\mathcal{H}_0|\Psi_{32}),$$

in which

$$\mathcal{H}_0=(p^2/2m)+V(\mathbf{r})+(\hbar^2\kappa^2/2m), \quad (13)$$

TABLE II. Decomposition of direct products of the type $S_i \times \Gamma_k \times S_j$.

Γ_1	S_1	S_2	S_3
S_1	Γ_1	Γ_2	Γ_3
S_2	Γ_2	Γ_1	Γ_3
S_3	Γ_3	Γ_3	$\Gamma_1+\Gamma_2+\Gamma_3$
Γ_2	S_1	S_2	S_3
S_1	Γ_2	Γ_1	Γ_3
S_2	Γ_1	Γ_2	Γ_3
S_3	Γ_3	Γ_3	$\Gamma_1+\Gamma_2+\Gamma_3$
Γ_3	S_1	S_2	S_3
S_1	Γ_3	Γ_3	$\Gamma_1+\Gamma_2+\Gamma_3$
S_2	Γ_3	Γ_3	$\Gamma_1+\Gamma_2+\Gamma_3$
S_3	$\Gamma_1+\Gamma_2+\Gamma_3$	$\Gamma_1+\Gamma_2+\Gamma_3$	$\Gamma_1+\Gamma_2+3\Gamma_3$

and κ is a wave vector in the $\mathbf{K}_1\mathbf{K}_2$ plane measured from the zone edge. The k_z dependence of the diagonal matrix elements is given explicitly at the end of this section.

Symmetry considerations can be used to show that certain matrix elements of the Hamiltonian must vanish, while other matrix elements are related one to another. Let $\mathcal{O}(\Gamma_k)$ be an operator which transforms according to the point group representation Γ_k, and $\Psi(S_i)$ be a wave function which transforms according to the group representation S_i. Then for matrix elements of the form $(\Psi(S_i)|\,\mathcal{O}(\Gamma_k)\,|\Psi(S_j))$ to be nonvanishing, it is necessary for the direct product $(S_i \times \Gamma_k \times S_j)$ to contain a Γ_1 in its decomposition, where Γ_1 is the identity representation for the point group derived from $G(S)$. Furthermore, the number of times that the representation Γ_1 is contained in such a decomposition is equal to the number of independent matrix elements of the form $(\Psi(S_i)|\,\mathcal{O}(\Gamma_k)\,|\Psi(S_j))$. Although the diagonal matrix elements are real, the off-diagonal terms are, in general, complex. But if the operator $\mathcal{O}$ is Hermitian, the off-diagonal matrix elements are related by complex conjugation. The direct products which enter into the evaluation of the matrix elements of Eqs. (9) and (10) are summarized in Table II. In this table, the representations Γ_k are listed in the upper left-hand corner of each block, the representations S_i in the left-hand column and the representations S_j in the top row. The results for the direct products are then tabulated as a matrix. Since the direct products $(S_i \times \Gamma_k \times S_j)$ for the operators $\mathcal{O}(\Gamma_k) = p_\pm$, $L_\pm$, L_z contain Γ_1 either once or not at all, there are at most three independent matrix elements for the "$\mathbf{k}\cdot\mathbf{p}$" Hamiltonian and five for the spin-orbit Hamiltonian. The relations between these matrix elements are found by performing the symmetry operations of the group and using the matrix representation given in Eq. (11) for the S_3 states. The matrix elements for the "$\mathbf{k}\cdot\mathbf{p}$" perturbation Hamiltonian taken between the spatial part of the wave functions are listed in Table III. The spin integration gives unity between states of like spin and zero otherwise. The k_z dependence

TABLE III. Matrix elements of the "$\mathbf{k}\cdot\mathbf{p}$" Hamiltonian. By time-reversal symmetry (see Appendix A), $\pi_{1,3}$, $\pi_{2,3}$, and $\pi_{3,3}$ are real.

$\mathcal{H}'$	Ψ_{11}	Ψ_{21}	Ψ_{31}	Ψ_{32}
Ψ_{11}	0	0	$\kappa_+\pi_{1,3}$	$\kappa_-\pi_{1,3}$
Ψ_{21}	0	0	$-\kappa_+\pi_{2,3}$	$\kappa_-\pi_{2,3}$
Ψ_{31}	$\kappa_-\pi_{1,3}^*$	$-\kappa_-\pi_{2,3}^*$	0	$\kappa_+\pi_{3,3}$
Ψ_{32}	$\kappa_+\pi_{1,3}^*$	$\kappa_+\pi_{2,3}^*$	$\kappa_-\pi_{3,3}$	0

of the independent matrix elements

$$\pi_{1,3}(k_z) = (\hbar/2m)(\Psi_{11}|\,p_-\,|\Psi_{31}) = (\hbar/2m)(\Psi_{11}|\,p_+\,|\Psi_{32}), \quad (14a)$$

$$\pi_{2,3}(k_z) = -(\hbar/2m)(\Psi_{21}|\,p_-\,|\Psi_{31}) = (\hbar/2m)(\Psi_{21}|\,p_+\,|\Psi_{32}), \quad (14b)$$

$$\pi_{3,3}(k_z) = (\hbar/2m)(\Psi_{31}|\,p_-\,|\Psi_{32}) = (\hbar/2m)(\Psi_{32}|\,p_+\,|\Psi_{31}) = \pi_{3,3}^*(k_z), \quad (14c)$$

is discussed at the end of this section. By using time-reversal symmetry (see Appendix A), the matrix elements $\pi_{1,3}$ and $\pi_{2,3}$ are also shown to be real. This "$\mathbf{k}\cdot\mathbf{p}$" Hamiltonian was derived by Slonczewski and Weiss[1] and discussed extensively by McClure.[11,12]

Whereas the "$\mathbf{k}\cdot\mathbf{p}$" Hamiltonian connects only the same spin states, the spin-orbit Hamiltonian terms $L_z\sigma_z$ couple the same spin states, while the $L_\pm\sigma_\mp$ terms couple opposite spin states. From the direct product decomposition given in Table II, it is seen that $(S_i \times \Gamma_2 \times S_j)$ contain Γ_1 three times; thus, there are two independent matrix elements of L_z, one of which is diagonal and the other off diagonal. Similarly, there are three other independent matrix elements involving $L_\pm$. The matrix elements for the spin-orbit Hamiltonian between states labeled by a spatial times a spin wave function are listed in Table IV, and are defined by

$$\lambda_{1,2}{}^z(k_z) = (\Psi_{11}|\,L_z\,|\Psi_{21}), \quad (15a)$$

$$\lambda_{3,3}{}^z(k_z) = (\Psi_{31}|\,L_z\,|\Psi_{31}) = -(\Psi_{32}|\,L_z\,|\Psi_{32}), \quad (15b)$$

$$\lambda_{1,3}(k_z) = (\Psi_{11}|\,L_-\,|\Psi_{31}) = (\Psi_{11}|\,L_+\,|\Psi_{32}), \quad (15c)$$

$$\lambda_{2,3}(k_z) = -(\Psi_{21}|\,L_-\,|\Psi_{31}) = (\Psi_{21}|\,L_+\,|\Psi_{32}), \quad (15d)$$

$$\lambda_{3,3}(k_z) = (\Psi_{31}|\,L_-\,|\Psi_{32}) = (\Psi_{32}|\,L_+\,|\Psi_{31}) = \lambda_{3,3}^*(k_z). \quad (15e)$$

The spatial symmetry of the graphite lattice gives the above relations for the matrix elements. In Appendix A it is shown by time-reversal symmetry that $\lambda_{1,2}{}^z$ is real, that $\lambda_{1,3}$ and $\lambda_{2,3}$ are pure imaginary, and that $\lambda_{3,3}$ vanishes identically. In Table IV, it is seen that the coupling between states of like spin only involves $L_z\sigma_z$ and that the matrix elements for $\mathcal{H}_{s.o.}$ between two spin-up states and two spin-down states are of opposite sign, which can be verified by carrying out the spin integration explicitly.

[11] J. W. McClure, Phys. Rev. **108**, 612 (1957).
[12] J. W. McClure, Phys. Rev. **119**, 606 (1960).

TABLE IV. Matrix elements of spin-orbit Hamiltonian. By time-reversal (see Appendix A) $\lambda_{1,2^z}$ $\lambda_{3,3^z}$ are real and $\lambda_{1,3}$ $\lambda_{2,3}$ are imaginary.

$\mathcal{H}_{s.o.}$	$\Psi_{11}\uparrow$	$\Psi_{21}\uparrow$	$\Psi_{31}\uparrow$	$\Psi_{32}\uparrow$	$\Psi_{11}\downarrow$	$\Psi_{21}\downarrow$	$\Psi_{31}\downarrow$	$\Psi_{32}\downarrow$
$\Psi_{11}\uparrow$	0	$\lambda_{1,2^z}$	0	0	0	0	$\lambda_{1,3}$	0
$\Psi_{21}\uparrow$	$\lambda_{1,2^{z*}}$	0	0	0	0	0	$-\lambda_{2,3}$	0
$\Psi_{31}\uparrow$	0	0	$\lambda_{3,3^z}$	0	0	0	0	0
$\Psi_{32}\uparrow$	0	0	0	$-\lambda_{3,3^z}$	$\lambda_{1,3}^*$	$\lambda_{2,3}^*$	0	0
$\Psi_{11}\downarrow$	0	0	0	$\lambda_{1,3}$	0	$-\lambda_{1,2^z}$	0	0
$\Psi_{21}\downarrow$	0	0	0	$\lambda_{2,3}$	$-\lambda_{1,2^{z*}}$	0	0	0
$\Psi_{31}\downarrow$	$\lambda_{1,3}^*$	$-\lambda_{2,3}^*$	0	0	0	0	$-\lambda_{3,3^z}$	0
$\Psi_{32}\downarrow$	0	0	0	0	0	0	0	$\lambda_{3,3^z}$

The k_z dependence of the matrix elements in Eqs. (12), (14), and (15) can be expressed as a Fourier cosine series in $k_z c_0/2$, where $c_0/2$ is the separation of adjacent atomic layers. Since the basal plane at $k_z=0$ is a reflection plane, all of the matrix elements are even functions of k_z and all terms in the Fourier sine series must vanish. In Appendix B it is shown that the wave functions which transform as the irreducible representations of the wave vector $\mathbf{k}_s$ have the following symmetry properties:

$$\Psi_{11}(\mathbf{k}_s \pm \mathbf{K}_4) = \Psi_{21}(\mathbf{k}_s), \tag{16a}$$

$$\Psi_{21}(\mathbf{k}_s \pm \mathbf{K}_4) = \Psi_{11}(\mathbf{k}_s), \tag{16b}$$

$$\Psi_{31}(\mathbf{k}_s \pm \mathbf{K}_4) = -\Psi_{31}(\mathbf{k}_s), \tag{16c}$$

$$\Psi_{32}(\mathbf{k}_s \pm \mathbf{K}_4) = \Psi_{32}(\mathbf{k}_s), \tag{16d}$$

in which $\mathbf{K}_4 = (2\pi/c_0)(0,0,1)$, and $\mathbf{k}_s$ defined by Eq. (4), is a function of k_z. Thus, the diagonal matrix elements defined by Eqs. (12) and (13) are written as

$$E_i(k_z) = (\hbar^2\kappa^2/2m) + E_i^0(k_z); \quad i=1,2,3, \tag{17a}$$

in which the terms $E_i^0(k_z)$ have the Fourier expansions

$$E_1^0(k_z) = \sum_{n=0}^{\infty} A_n \cos(n\pi\xi), \tag{17b}$$

$$E_2^0(k_z) = \sum_{n=0}^{\infty} A_n(-1)^n \cos(n\pi\xi), \tag{17c}$$

$$E_3^0(k_z) = \sum_{n=0}^{\infty} B_n \cos(2n\pi\xi), \tag{17d}$$

and the dimensionless wave vector ξ is defined by $\xi = k_z c_0/2\pi$. To obtain Eqs. (17), the relations of Eq. (16) have been used to relate the Fourier coefficients in the expansions for E_1^0 and E_2^0 and to cancel the odd terms in the expansion for E_3^0. The terms in κ^2 given in Eq. (17a) are generally neglected, but are of about the same magnitude as the spin-orbit terms that have been included.

Similarly, the Eqs. (14) can be expanded to give

$$\pi_{1,3}(k_z) = \sum_{n=0}^{\infty} C_n \cos(n\pi\xi), \tag{18a}$$

$$\pi_{2,3}(k_z) = \sum_{n=0}^{\infty} C_n(-1)^n \cos(n\pi\xi), \tag{18b}$$

$$\pi_{3,3}(k_z) = \sum_{n=0}^{\infty} D_n \cos([2n+1]\pi\xi), \tag{18c}$$

and Eqs. (15) can be expanded to give

$$\lambda_{1,2^z}(k_z) = \sum_{n=0}^{\infty} F_n \cos(2n\pi\xi), \tag{19a}$$

$$\lambda_{3,3^z}(k_z) = \sum_{n=0}^{\infty} G_n \cos(2n\pi\xi), \tag{19b}$$

$$\lambda_{1,3}(k_z) = i \sum_{n=0}^{\infty} H_n \cos(n\pi\xi), \tag{19c}$$

$$\lambda_{2,3}(k_z) = i \sum_{n=0}^{\infty} H_n(-1)^n \cos(n\pi\xi). \tag{19d}$$

In these equations the Fourier coefficients A_n, B_n, C_n, D_n, F_n, G_n, H_n are shown in Appendix A to be real. The relation between the A_n, B_n, C_n, and D_n coefficients and the band parameters defined by McClure[11] are summarized in Table V. In constructing this table, the Fourier expansions in Eqs. (17) and (19) were cut off in a manner consistent with the number of terms retained by McClure.

McClure has shown how these band parameters can be related to overlap integrals involving tight binding functions.[11] Furthermore, McClure and Yafet[7] have discussed a tight binding calculation of the $\lambda_{1,2^z}$ and $\lambda_{3,3^z}$ matrix elements. They point out that with the

TABLE V. Relation between Fourier coefficients and McClure's band parameters.

McClure band parameters	Fourier coefficients
γ_0	$-\mu C_0$
γ_1	$A_1/2$
γ_2	B_1
γ_3	$\mu D_0\sqrt{2}/4$
γ_4	$\mu C_1/2$
γ_5	A_2
Δ	$A_0-A_2-B_0+B_1$

where $\mu = 2(6)^{1/2}/3a_0$

tight binding functions given in Eqs. (A1) and (A2), which depend only on $2p_z$ orbitals, the expressions for the larger magnitude spin-orbit matrix elements (i.e., $\lambda_{1,2}{}^z$ and $\lambda_{3,3}{}^z$) depend on two-center integrals, whereas the terms of smaller magnitude (i.e., $\lambda_{1,3}$ and $\lambda_{2,3}$) depend on three-center integrals. The tight-binding estimates of McClure and Yafet show that the admixture of d functions into the wave functions with S_1, S_2, and S_3 symmetry produces a larger contribution to the spin-orbit matrix elements than the overlaps of the $2p_z$ functions. The tight binding arguments of McClure and Yafet could be used to calculate the magnitude of all the spin-orbit matrix elements required by symmetry. In this paper, no such tight binding calculation has been made and the evaluation of the spin-orbit matrix elements is left to experiment. The tight binding arguments indicate that for graphite only the leading terms F_0, G_0, and H_0 need be considered. Thus, there are three spin-orbit band parameters to be evaluated by experiment.

The generality of the graphite effective-mass Hamiltonian was appreciated by McClure and others, and used explicitly in the experimental determination of the graphite band parameters.[7,11–13] Since this derivation only employs the symmetry of a hexagonal lattice, the effective-mass Hamiltonian for any hexagonal material near the edge of the Brillouin zone can be related to this graphite Hamiltonian.

III. GRAPHITE FERMI SURFACE

In this section the energy eigenvalues for the graphite effective-mass Hamiltonian are found and the results are applied to calculate the areas and effective masses for Fermi-surface cross sections normal to the c axis. It is seen that even though the spin-orbit band parameters might be small, they are nevertheless important in lifting energy band degeneracies (1) at the Brillouin-zone vertical edges, (2) at the Brillouin-zone boundaries $k_z=\pm\pi/c_0$, and (3) at the intersection of the edges with the planes, i.e., points H and H'.

The energy eigenvalues are found by solution of the secular equation derived from the graphite effective-mass Hamiltonian discussed in the previous section:

$$\begin{vmatrix} e_1 & \lambda_{1,2}{}^z & H_{13} & H_{13}{}^* & 0 & 0 & \lambda_{1,3} & 0 \\ \lambda_{1,2}{}^z & e_2 & H_{23} & -H_{23}{}^* & 0 & 0 & -\lambda_{2,3} & 0 \\ H_{13}{}^* & H_{23}{}^* & e_3+\lambda_{3,3}{}^z & H_{33} & 0 & 0 & 0 & 0 \\ H_{13} & -H_{23} & H_{33}{}^* & e_3-\lambda_{3,3}{}^z & -\lambda_{1,3} & -\lambda_{2,3} & 0 & 0 \\ 0 & 0 & 0 & \lambda_{1,3} & e_1 & -\lambda_{1,2}{}^z & H_{13} & H_{13}{}^* \\ 0 & 0 & 0 & \lambda_{2,3} & -\lambda_{1,2}{}^z & e_2 & H_{23} & -H_{23}{}^* \\ -\lambda_{1,3} & \lambda_{2,3} & 0 & 0 & H_{13}{}^* & H_{23}{}^* & e_3-\lambda_{3,3}{}^z & H_{33} \\ 0 & 0 & 0 & 0 & H_{13} & -H_{23} & H_{33}{}^* & e_3+\lambda_{3,3}{}^z \end{vmatrix} = 0 \tag{20}$$

in which e_i is related to the energy eigenvalue ϵ by

$$e_i=E_i-\epsilon; \quad i=1, 2, 3, \tag{21}$$

and the notation

$$H_{13}=\kappa_+\pi_{1,3}, \tag{22a}$$

$$H_{23}=-\kappa_+\pi_{2,3}, \tag{22b}$$

$$H_{33}=\kappa_+\pi_{3,3}, \tag{22c}$$

is used. The matrix elements $\pi_{1,3}$, $\pi_{2,3}$, and $\pi_{3,3}$, $\lambda_{1,2}{}^z$, $\lambda_{3,3}{}^z$ are real while the matrix elements $\lambda_{1,3}$ and $\lambda_{2,3}$ are imaginary. The determinantal secular equation can be multiplied out—for example, by using the method of Laplace on the 4×4 blocks for like and unlike spins. The result is

$$[|H_{1,2,3,4}{}^{1,2,3,4}|-|\lambda_{1,3}|^2\{e_2(e_3+\lambda_{3,3}{}^z)-|H_{23}|^2\}-|\lambda_{2,3}|^2\{e_1(e_3+\lambda_{3,3}{}^z)-|H_{13}|^2\} -2|\lambda_{1,3}||\lambda_{2,3}|\{\lambda_{1,2}{}^z(e_3+\lambda_{3,3}{}^z)-H_{13}H_{23}{}^*\}]^2=0, \tag{23}$$

in which the 4×4 block coupling like spins is

$$|H_{1,2,3,4}{}^{1,2,3,4}|=\{e_1e_2-(\lambda_{1,2}{}^z)^2\}\{e_3{}^2-(\lambda_{3,3}{}^z)^2\}-\{e_1e_2|H_{33}|^2+2e_1e_3|H_{23}|^2+2e_2e_3|H_{13}|^2\} -\{e_1(H_{23}{}^2H_{33}+H_{23}{}^{*2}H_{33}{}^*)-e_2(H_{13}{}^2H_{33}+H_{13}{}^{*2}H_{33}{}^*)\}+4|H_{13}|^2|H_{23}|^2+(\lambda_{1,2}{}^z)^2|H_{33}|^2-4\lambda_{3,3}{}^z\lambda_{1,2}{}^zH_{13}H_{23}{}^*. \tag{24}$$

The factorization of this 8th-order equation in ϵ into two identical quartic equations implies a double degeneracy of all the energies, which is consistent with the time reversal requirements of group theory. In the presence of a magnetic field, this time reversal degeneracy is lifted and no such factorization of the Hamiltonian is possible.

For a general point in the Brillouin zone, where there

[13] M. S. Dresselhaus and J. G. Mavroides, IBM J. Res. Develop. 8, 262 (1964).

are no band degeneracies, the spin-orbit terms can be neglected and the quartic equation can be solved for the energy eigenvalues. However, at the three Brillouin-zone locations having band degeneracies, the solution of Eq. (23) must be carried out in more detail.

At the zone edge, Eq. (23) reduces to

$$[e_3+\lambda_{3,3}{}^z][\{e_1e_2-(\lambda_{1,2}{}^z)^2\}\{e_3-\lambda_{3,3}{}^z\} - |\lambda_{1,3}|^2e_2-|\lambda_{2,3}|^2e_1-2|\lambda_{1,3}||\lambda_{2,3}|\lambda_{1,2}{}^z]=0. \quad (25)$$

Thus, the degeneracy of the E_3 bands is lifted at the zone edge. Neglecting $|\lambda_{1,3}|$ and $|\lambda_{2,3}|$, as suggested by the tight binding arguments of McClure and Yafet,[7] the band splitting shown in Fig. 3 is obtained for a general point along the zone edges HKH and $H'K'H'$, but not in the vicinity of the zone corners H and H'. The E_1 and E_2 levels are only shifted slightly, i.e., of order $(\lambda_{1,2}{}^z)^2/(E_1-E_2)$, while the E_3 bands are split by $2\lambda_{3,3}{}^z$.

In the absence of spin-orbit interaction, the planes $\xi=\pm\frac{1}{2}$ exhibit two sets of doubly degenerate bands, with energies $\frac{1}{2}(E_1\pm\{E_1{}^2+8|H_{13}|^2\}^{1/2})$, since $E_1=E_2$. These degeneracies are again lifted by the spin-orbit interaction and at $\xi=\pm\frac{1}{2}$, Eq. (23) reduces to

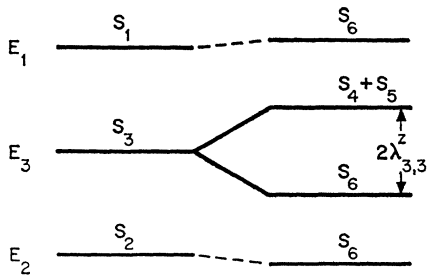

FIG. 3. The effect of spin-orbit interaction on the energy bands at the zone edge. In the absence of spin-orbit interaction the bands are labeled using the conventional notation and the irreducible representations corresponding to these bands are indicated. With spin-orbit interaction, the resulting bands are labeled by the double group representation.

$$\{(e_1+\lambda_{1,2}{}^z)(e_3+\lambda_{3,3}{}^z)-2|H_{13}|^2\}=0, \quad (26a)$$

$$\{(e_1-\lambda_{1,2}{}^z)(e_3-\lambda_{3,3}{}^z)-2|H_{13}|^2-2|\lambda_{1,3}|^2\}=0, \quad (26b)$$

in which the equality $|\lambda_{1,3}|=|\lambda_{2,3}|$ at $\xi=\frac{1}{2}$ has been used. Equation (26) has the roots

$$\epsilon=\tfrac{1}{2}[E_1+\lambda_{1,2}{}^z+\lambda_{3,3}{}^z\pm\{(E_1+\lambda_{1,2}{}^z-\lambda_{3,3}{}^z)^2+8|H_{13}|^2\}^{1/2}], \quad (27a)$$

$$\epsilon=\tfrac{1}{2}[E_1-\lambda_{1,2}{}^z-\lambda_{3,3}{}^z\pm\{(E_1-\lambda_{1,2}{}^z+\lambda_{3,3}{}^z)^2+8|H_{13}|^2+8|\lambda_{1,3}|^2\}^{1/2}]. \quad (27b)$$

The twofold degeneracy in this plane is lifted by the spin-orbit interaction. These band splittings are indicated in Fig. 4, using the approximations suggested by McClure and Yafet,[7] $\lambda_{3,3}{}^z\approx\lambda_{1,2}{}^z$ and $|\lambda_{1,3}|=0$. The effect of the off-diagonal matrix element $|\lambda_{1,3}|$ is to make the band splittings unequal. The κ dependence of the energy bands in this plane is obtained explicitly by the substitution $E_1=\Delta+(\hbar^2\kappa^2/2m)$ and $|H_{13}|^2=\frac{3}{8}\gamma_0{}^2a_0{}^2\kappa^2$.

At the zone corners, H and H', both the degeneracies of the zone edges and zone boundaries are present in the absence of spin-orbit interaction. These degeneracies are lifted according to Eqs. (27) as $|H_{13}|\to 0$. Since at the zone corner in graphite $E_1=\Delta<0$, the energy of the band derived from $\frac{1}{2}(E_1+\{E_1{}^2+8|H_{13}|^2\}^{1/2})$ is lower than that from $\frac{1}{2}(E_1-\{E_1{}^2+8|H_{13}|^2\}^{1/2})$. The splitting pattern at the zone corner is shown in Fig. 5, using the same approximations as in constructing Fig. 4. The effect of the matrix element $|\lambda_{1,3}|$ is to produce equal and opposite shifts in two of the levels.

Thus, it is seen that all band degeneracies at these three locations in the Brillouin zone are lifted by the spin-orbit interaction terms connecting states of like spins. The matrix elements connecting unlike spins are relatively less important and effectively contribute only to the asymmetry of the splittings. These results are consistent with the McClure-Yafet approximation of neglecting matrix elements connecting unlike spins in their calculation of the g shift in graphite.[7]

Although the off-diagonal matrix elements $\lambda_{1,3}$ and $\lambda_{2,3}$ are relatively unimportant in determining the energy levels at critical points in the Brillouin zone, these matrix elements are quite important in determining the properties of the Fermi surface at the zone boundary. The Fermi surface cross-sectional area can be found from solution of Eq. (23) for $|\kappa|^2=\kappa_+\kappa_-$, which is rewritten as

$$B_4|\kappa|^4+B_3\cos3\theta|\kappa|^3+B_2|\kappa|^2+B_0=0, \quad (28)$$

in which $\kappa_\pm=|\kappa|e^{\pm i\theta}$ and the coefficients are

$$B_4=4\pi_{1,3}{}^2\pi_{2,3}{}^2, \quad (29a)$$

$$B_3=2\pi_{3,3}\{e_2\pi_{1,3}{}^2-e_1\pi_{2,3}{}^2\}, \quad (29b)$$

$$B_2=-\pi_{3,3}{}^2\{e_1e_2-(\lambda_{1,2}{}^z)^2\} -\pi_{1,3}{}^2\{2e_2e_3-|\lambda_{2,3}|^2\}-\pi_{2,3}{}^2\{2e_1e_3-|\lambda_{1,3}|^2\} +2\pi_{1,3}\pi_{2,3}\{2\lambda_{3,3}{}^z\lambda_{1,2}{}^z-|\lambda_{1,3}||\lambda_{2,3}|\}, \quad (29c)$$

$$B_0=\{e_3+\lambda_{3,3}{}^z\}\{[e_1e_2-(\lambda_{1,2}{}^z)^2][e_3-\lambda_{3,3}{}^z] -e_2|\lambda_{1,3}|^2-e_1|\lambda_{2,3}|^2-2|\lambda_{1,3}||\lambda_{2,3}|\lambda_{1,2}{}^z\}. \quad (29d)$$

For simplicity, the small terms $\hbar^2\kappa^2/2m$ in the energies e_i have been neglected. Provided that the Fermi surface is simply connected, the Fermi surface cross section normal to the c axis is found by performing the integral

$$S=3\int_0^{\pi/3}|\kappa_F|^2d\theta, \quad (30)$$

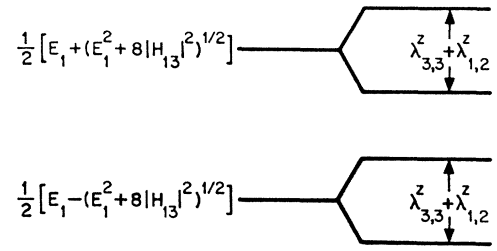

FIG. 4. The effect of spin-orbit interaction on the energy bands at the zone boundary, defined by the planes $\xi=\pm\frac{1}{2}$.

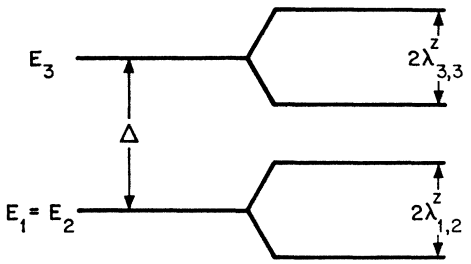

FIG. 5. The effect of spin-orbit interaction on the energy bands at the zone corners, H and H'.

in which the wave vector $|\kappa_F|$ is evaluated from solution of Eq. (28) at the Fermi energy $\epsilon=E_F$. For a general value of k_z no band degeneracies are involved, and spin-orbit interaction is relatively unimportant. In that case, most of the Fermi surface can be constructed from Eq. (30) using measured values of the band parameters, as is done, for example, in Ref. 13.

However, at $k_z=\pi/c_0$, spin-orbit interaction is important in lifting the degeneracy of the Fermi-surface cross section at the zone boundary. It is this area which has recently been investigated by Soule[4] and Williamson *et al.*[5] in studies of the low-frequency de Haas–van Alphen oscillations in single-crystal and pyrolytic graphite. In this special case the coefficients in Eq. (29) become

$$B_4=4\pi_{1,3}{}^4, \tag{31a}$$

$$B_3=0, \tag{31b}$$

$$B_2=-4\pi_{1,3}{}^2(e_1e_3-\lambda_{3,3}{}^z\lambda_{1,2}{}^z), \tag{31c}$$

$$B_0=(e_3+\lambda_{3,3}{}^z)(e_1+\lambda_{1,2}{}^z)\times\{(e_1-\lambda_{1,2}{}^z)(e_3-\lambda_{3,3}{}^z)-2|\lambda_{1,3}|^2\}. \tag{31d}$$

Since the term in $|\kappa|^3$ vanishes, Eq. (28) becomes quadratic in $|\kappa|^2$ and has solutions at the Fermi surface denoted by $|\kappa_F|^2$. Thus, the cross-sectional area $S=\pi|\kappa_F|^2$ at the plane $\xi=\frac{1}{2}$ can be written as

$$S=S_0\left[1-\frac{\lambda_{3,3}{}^z\lambda_{1,2}{}^z}{E_F(E_F-\Delta)}\pm\frac{\Omega^2}{E_F(E_F-\Delta)}\right] \tag{32}$$

in which the Fermi-surface cross section without spin-orbit interaction in terms of the McClure graphite energy-band parameters is

$$S_0=4\pi E_F(E_F-\Delta)/3\gamma_0{}^2a_0{}^2 \tag{33}$$

and the spin-orbit term Ω, which has the dimensions of energy, is defined by

$$\Omega^2=[(e_1\lambda_{3,3}{}^z-e_3\lambda_{1,2}{}^z)^2+2|\lambda_{1,3}|^2(e_3+\lambda_{3,3}{}^z)(e_1+\lambda_{1,2}{}^z)]^{1/2}. \tag{34}$$

If the approximation $|\lambda_{1,3}|=0$ is made, Eq. (32) simplifies to

$$S\cong S_0\left(1\mp\frac{\lambda_{1,2}{}^z}{E_F-\Delta}\right)\left(1\pm\frac{\lambda_{3,3}{}^z}{E_F}\right). \tag{35}$$

The lifting of the degeneracy of the Fermi-surface cross section at the zone boundary implies that two nearly equal low-frequency de Haas–van Alphen oscillations should be observed, and, in fact, preliminary results by Soule[4] indicate the existence of two such oscillations in single-crystal graphite. Since in pyrolytic graphite[3] $2E_F(E_F-\Delta)\gg\Delta^2$, it is expected that the off-diagonal matrix elements $\lambda_{1,3}$ and $\lambda_{2,3}$ are of some importance in determined the splittings of the degenerate Fermi-surface cross section and the complete expression given by Eq. (32) is applicable.

The cyclotron effective masses corresponding to these Fermi surface cross sections are found by performing the integral

$$m^*=\frac{3\hbar^2}{\pi}\int_0^{\pi/3}|\kappa|\left(\frac{\partial E}{\partial|\kappa|}\right)^{-1}d\theta, \tag{36a}$$

in which the angular dependence of $|\kappa|$ and $\partial E/\partial|\kappa|$ at the Fermi surface are found by appropriate solution of Eq. (28). At the zone boundary, $\xi=\frac{1}{2}$, there is no angular dependence for $|\kappa|$ and $\partial E/\partial|\kappa|$, so that an explicit expression for m^* can be written

$$m^*=m_0{}^*\left\{1\mp\frac{(e_1\lambda_{3,3}{}^z-e_3\lambda_{1,2}{}^z)(\lambda_{3,3}{}^z-\lambda_{1,2}{}^z)+|\lambda_{1,3}|^2(e_1+e_3+\lambda_{3,3}{}^z+\lambda_{1,2}{}^z)}{(2E_F-\Delta)\Omega^2}\right\}, \tag{36b}$$

in which the effective mass in the absence of spin-orbit interaction $m_0{}^*$ is

$$m_0{}^*=2\hbar^2(2E_F-\Delta)/3\gamma_0{}^2a_0{}^2. \tag{37}$$

Since $\lambda_{3,3}{}^z\approx\lambda_{1,2}{}^z$, the terms in the off-diagonal matrix element $|\lambda_{1,3}|$ are important in lifting the degeneracy in the effective mass, with the larger m^* being associated with the larger cross-sectional area. Numerical values of the spin-orbit band parameters could, in principle, be found by detailed analysis of the two nearly degenerate

de Haas–van Alphen oscillations, of their temperature dependence, and of their anisotropy.

IV. EFFECTIVE-MASS HAMILTONIAN IN A MAGNETIC FIELD

In this section the effective-mass Hamiltonian in the presence of a magnetic field is derived and is applied to study the effect of spin-orbit interaction on the magnetoreflection experiment. The magnetic Hamiltonian is generated from the zero-field Hamiltonian by the transcription $\boldsymbol{\kappa} \rightarrow \boldsymbol{\kappa} - e\mathbf{A}/c\hbar$ and the gauge for the static magnetic field $\mathbf{H}$ is selected as $\mathbf{A}=(0, Hx, 0)$. This treatment is a generalization of the McClure-Inoue equation,[12,14] which has been useful in the analysis of the diamagnetic susceptibility[12] and magnetoreflection experiments.[13] The (8×8) Hamiltonian can be written in the form $\mathbf{H}=\mathbf{H}_0+\mathbf{H}'$ in which

$$\mathbf{H}_0=\begin{pmatrix}\mathfrak{D}_+ & \mathfrak{L}\\ \mathfrak{L}^\dagger & \mathfrak{D}_-\end{pmatrix}, \tag{38}$$

where the (4×4) matrices $\mathfrak{D}_\pm$ and $\mathfrak{L}$ are defined by

$$\mathfrak{D}_\pm=\begin{bmatrix} E_1\pm\mu H & \pm\lambda_{1,2}{}^z & H_{13} & H_{13}{}^* \\ \pm\lambda_{1,2}{}^z & E_2\pm\mu H & H_{23} & -H_{23}{}^* \\ H_{13}{}^* & H_{23}{}^* & E_3\pm\lambda_{3,3}{}^z\pm\mu H & 0 \\ H_{13} & -H_{23} & 0 & E_3\mp\lambda_{3,3}{}^z\pm\mu H \end{bmatrix} \tag{39}$$

and

$$\mathfrak{L}=\begin{bmatrix} 0 & 0 & \lambda_{1,3} & 0 \\ 0 & 0 & -\lambda_{2,3} & 0 \\ 0 & 0 & 0 & 0 \\ -\lambda_{1,3} & -\lambda_{2,3} & 0 & 0 \end{bmatrix}. \tag{40}$$

The Hamiltonian $\mathbf{H}_0$ is exactly diagonalized by the eight-component effective-mass wave function $\Psi_{n,j}$ which can be written in the form

$$\Psi_{n,j}=(1/2\pi)e^{i\kappa_z z}e^{i\kappa_y y}\Phi_{n,j}, \tag{41a}$$

in which $\Phi_{n,j}$ can be represented by a vector with 8 components which for $n\geqslant 1$ can be written as

$$\Phi_{n,j}=(C_{1+}{}^{n,j}\psi_n, C_{2+}{}^{n,j}\psi_n, C_{31+}{}^{n,j}\psi_{n-1}, C_{32+}{}^{n,j}\psi_{n+1}, C_{1-}{}^{n,j}\psi_{n+1}, C_{2-}{}^{n,j}\psi_{n+1}, C_{31-}{}^{n,j}\psi_n, C_{32-}{}^{n,j}\psi_{n+2}). \tag{41b}$$

Here the ψ_n are normalized harmonic-oscillator functions centered at $[x-(c\hbar\kappa_y/eH)]$. For a given "oscillator state" n there are eight eigenstates and eigenvalues, labeled by j. The terms H_{13} and H_{23}, defined by Eqs. (22a) and (22b), are now operators. The matrix elements $\pi_{1,3}$ and $\pi_{2,3}$ are real, and the raising operator κ_+ and the lowering operator κ_- acting on the harmonic-oscillator wave functions yield

$$\kappa_+\psi_n=[(n+1)s]^{1/2}\psi_{n+1}, \tag{42a}$$

$$\kappa_-\psi_n=[ns]^{1/2}\psi_{n-1}, \tag{42b}$$

in which

$$s=2|e|H/c\hbar. \tag{42c}$$

The effective-mass wave functions $\Psi_{n,j}$ for the special cases $n=0, -1, -2$ are found from Eq. (41) by setting the coefficient $C_i{}^{n,j}=0$ whenever the associated-harmonic-oscillator quantum number is negative, e.g., $C_{31+}{}^{n,j}=0$, for $n=0, -1, -2$.

The secular equation which determines the magnetic energy levels for $n>1$ is given by

$$\begin{vmatrix} \mathfrak{B}_+(n) & \mathfrak{L} \\ \mathfrak{L}^\dagger & \mathfrak{B}_-(n+1) \end{vmatrix}=0, \tag{43}$$

in which the 4×4 matrix $\mathfrak{B}_\pm(n)$ is defined by

$$\mathfrak{B}_\pm(n)=\begin{bmatrix} e_{1\pm}(n) & \pm\lambda_{1,2}{}^z & (ns)^{1/2}\pi_{1,3} & ((n+1)s)^{1/2}\pi_{1,3} \\ \pm\lambda_{1,2}{}^z & e_{2\pm}(n) & -(ns)^{1/2}\pi_{2,3} & ((n+1)s)^{1/2}\pi_{2,3} \\ (ns)^{1/2}\pi_{1,3} & -(ns)^{1/2}\pi_{2,3} & e_{31\pm}(n) & 0 \\ ((n+1)s)^{1/2}\pi_{1,3} & ((n+1)s)^{1/2}\pi_{2,3} & 0 & e_{32\pm}(n) \end{bmatrix} \tag{44}$$

and

$$e_{i\pm}(n)=E_i{}^0\pm\mu H+(\hbar^2 s/2m)(n+\tfrac{1}{2})-\epsilon; \quad i=1, 2, \tag{45a}$$

$$e_{31\pm}(n)=E_3{}^0\pm\mu H\pm\lambda_{3,3}{}^z+(\hbar^2 s/2m)(n-\tfrac{1}{2})-\epsilon, \tag{45b}$$

$$e_{32\pm}(n)=E_3{}^0\pm\mu H\mp\lambda_{3,3}{}^z+(\hbar^2 s/2m)(n+\tfrac{3}{2})-\epsilon. \tag{45c}$$

The matrix $\mathbf{H}'$ is given by

$$\mathbf{H}'=\begin{pmatrix}\mathfrak{D}' & \mathfrak{O}\\ \mathfrak{O} & \mathfrak{D}'\end{pmatrix}, \tag{46}$$

in which

$$\mathfrak{D}'=\begin{bmatrix} 0 & 0 & 0 & 0 \\ 0 & 0 & 0 & 0 \\ 0 & 0 & 0 & H_{33} \\ 0 & 0 & H_{33}{}^* & 0 \end{bmatrix}, \tag{47}$$

and $\mathfrak{O}$ is the 4×4 zero matrix. The matrix $\mathbf{H}'$ is not diagonal in $\Psi_{n,j}$, but couples the states n to $n\pm 3$. The

[14] M. Inoue, J. Phys. Soc. Japan **17**, 808 (1962).

nonvanishing matrix elements of $\mathbf{H}'$ in the representation which diagonalizes $\mathbf{H}_0$ are

$$(\Phi_{n+3,j'}|\,\mathbf{H}'\,|\Phi_{n,j})=s^{1/2}\pi_{3,3}[C_{31+}{}^{n+3,j'*}C_{32+}{}^{n,j}(n+2)^{1/2}+C_{31-}{}^{n+3,j'*}C_{32-}{}^{n,j}(n+3)^{1/2}], \tag{48a}$$

$$(\Phi_{n-3,j'}|\,\mathbf{H}'\,|\Phi_{n,j})=s^{1/2}\pi_{3,3}[C_{32+}{}^{n-3,j'*}C_{31+}{}^{n,j}(n-1)^{1/2}+C_{32-}{}^{n-3,j'*}C_{31-}{}^{n,j}n^{1/2}]. \tag{48b}$$

The magnetic energy levels $E_{n,j}(j=1,\cdots 8)$ are calculated by solution of the secular equation defined by Eq. (43). The corrections to these levels associated with the trigonal warping band parameter γ_3 are found by treating $\mathbf{H}'$ in second-order perturbation theory. The effect of the magnetic field is to lift the Kramers degeneracy and to produce nondegenerate Landau levels. For a general value of k_z, there are eight Landau ladders, four of which are essentially spin up, and four spin down. Because of the complexity of the (8×8) Hamiltonian, explicit solutions for these energy levels must be found, in general, by machine calculation using band parameters determined from experiment.

However at $\xi=\frac{1}{2}$, a relatively simple solution can be found and the effect of spin-orbit interaction is to lift all the degeneracies implicit in the McClure-Inoue solution[12,14] at the zone corner

$$\epsilon_n=(\Delta/2)\pm[(\Delta/2)^2+(n,\,n+1)\tfrac{3}{4}s\gamma_0{}^2a_0{}^2]^{1/2}. \tag{49}$$

When spin-orbit interaction is included, the magnetic secular determinant given by Eq. (43) factors to give two quartic equations given by

$$\{2[h(n)]^2-e_{31+}(n)[e_{1+}(n)-\lambda_{1,2}{}^z]\}\times\{2[h(n+1)]^2-e_{31-}(n+1)[e_{1-}(n+1)+\lambda_{1,2}{}^z]\}=-2|\lambda_{1,3}|^2e_{31+}(n)[e_{1-}(n+1)+\lambda_{1,2}{}^z] \tag{50a}$$

and

$$\{2[h(n+1)]^2-e_{32+}(n)[e_{1+}(n)+\lambda_{1,2}{}^z]\}\times\{2[h(n+2)]^2-e_{32-}(n+1)[e_{1-}(n+1)-\lambda_{1,2}{}^z]\}=-2|\lambda_{1,3}|^2e_{32-}(n+1)[e_{1+}(n)+\lambda_{1,2}{}^z], \tag{50b}$$

in which

$$h(n)=(ns)^{1/2}\pi_{1,3}. \tag{50c}$$

If the electron-spin terms and the free-electron term $\hbar^2\kappa^2/2m$ are ignored, these equations at $\xi=\frac{1}{2}$ (point H in the Brillouin zone) reduce to the simple result given by McClure,[12] Eq. (49). The effect of spin-orbit interaction is to lift all the degeneracies at point H. The results for the eight energy levels, neglecting the small correction arising from terms in $|\lambda_{1,3}|^2$, are $\epsilon_n{}^{\pm}(1,1,1)$, $\epsilon_{n+1}{}^{\pm}(-1,-1,1)$, $\epsilon_{n+1}{}^{\pm}(1,-1,-1)$, and $\epsilon_{n+2}{}^{\pm}(-1,1,-1)$, in which the function $\epsilon_n{}^{\pm}(\alpha,\beta,\gamma)$ is defined by

$$\epsilon_n{}^{\pm}(\alpha,\beta,\gamma)=\Delta/2+\alpha\mu H+\beta(\lambda_{3,3}{}^z-\lambda_{1,2}{}^z)/2+(\hbar^2s/2m)n\pm\tfrac{1}{2}[\{\Delta+(\gamma\hbar^2s/2m)-\beta(\lambda_{3,3}{}^z+\lambda_{1,2}{}^z)\}^2+3ns\gamma_0{}^2a_0{}^2]^{1/2}. \tag{51}$$

These energy levels at $\xi=\frac{1}{2}$ are of particular interest in the analysis of the low-frequency de Haas–van Alphen oscillations and the oscillatory magnetoreflection experiments.

In these magnetoreflection experiments, electronic transitions between magnetic energy levels are induced by application of optical electromagnetic fields. The Hamiltonian describing the optical perturbation is

$$\mathbf{H}_{op}{}'=\begin{pmatrix}\mathfrak{D}_{op} & 0\\ 0 & \mathfrak{D}_{op}\end{pmatrix}. \tag{52}$$

The matrix $\mathfrak{D}_{op}$ depends on $A^{\pm}$, the vector potential for right and left circularly polarized light, through

$$\mathfrak{D}_{op}=-(e/hc)[A^+\mathfrak{D}_{op}{}^-+A^-\mathfrak{D}_{op}{}^+], \tag{53}$$

in which the 4×4 matrices $\mathfrak{D}_{op}{}^{\pm}$ are given by

$$\mathfrak{D}_{op}{}^-=\begin{bmatrix}(\hbar^2/2m)\kappa_- & 0 & \pi_{1,3} & 0\\ 0 & (\hbar^2/2m)\kappa_- & -\pi_{2,3} & 0\\ 0 & 0 & (\hbar^2/2m)\kappa_- & \pi_{3,3}\\ \pi_{1,3} & \pi_{2,3} & 0 & (\hbar^2/2m)\kappa_-\end{bmatrix} \tag{54}$$

and $\mathfrak{D}_{op}{}^+$ is the Hermitian transpose of $\mathfrak{D}_{op}{}^-$. The selection rules for optical transitions are found by looking for the nonvanishing matrix elements of the form $(\Phi_{n',j'}|\,\mathbf{H}_{op}{}'|\,\Phi_{n,j})$,

$$\begin{aligned}(\Phi_{n-1,j'}|\,\mathfrak{D}_{op}{}^-|\,\Phi_{n,j})=&\pi_{1,3}[C_{1+}{}^{n-1,j'*}C_{31+}{}^{n,j}+C_{32+}{}^{n-1,j'*}C_{1+}{}^{n,j}+C_{1-}{}^{n-1,j'*}C_{31-}{}^{n,j}+C_{32-}{}^{n-1,j'*}C_{1-}{}^{n,j}]\\&+\pi_{2,3}[-C_{2+}{}^{n-1,j'*}C_{31+}{}^{n,j}+C_{32+}{}^{n-1,j'*}C_{2+}{}^{n,j}-C_{2-}{}^{n-1,j'*}C_{31-}{}^{n,j}+C_{32-}{}^{n-1,j'*}C_{2-}{}^{n,j}]\\&+(\hbar^2/2m)s^{1/2}[n^{1/2}(C_{1+}{}^{n-1,j'*}C_{1+}{}^{n,j}+C_{2+}{}^{n-1,j'*}C_{2+}{}^{n,j}+C_{31-}{}^{n-1,j'*}C_{31-}{}^{n,j})\\&+(n+1)^{1/2}(C_{32+}{}^{n-1,j'*}C_{32+}{}^{n,j}+C_{1-}{}^{n-1,j'*}C_{1-}{}^{n,j}+C_{2-}{}^{n-1,j'*}C_{2-}{}^{n,j})\\&+(n-1)^{1/2}C_{31+}{}^{n-1,j'*}C_{31+}{}^{n,j}+(n+2)^{1/2}C_{32-}{}^{n-1,j'*}C_{32-}{}^{n,j}]\end{aligned} \tag{55}$$

and

$$(\Phi_{n+2,j'}|\,\mathfrak{D}_{op}{}^-|\,\Phi_{n,j})=\pi_{3,3}[C_{31+}{}^{n+2,j'*}C_{32+}{}^{n,j}+C_{31-}{}^{n+2,j'*}C_{32-}{}^{n,j}]. \tag{56}$$

The nonvanishing matrix elements for the other sense of circular polarization can be found from Eqs. (55) and (56) by making use of the relation

$$(\Phi_{n,j}|\,\mathfrak{D}_{\rm op}^{-}\,|\Phi_{n',j'})=(\Phi_{n',j'}|\,\mathfrak{D}_{\rm op}^{+}\,|\Phi_{n,j}). \quad (57)$$

Thus, the selection rule for allowed optical transitions is $\Delta n=\pm 1$ on the effective-mass wave functions $\Psi_{n,j}$, whether or not spin-orbit interaction is included. The interpretation of this selection rule is somewhat different than that for simple parabolic uncoupled bands where $\Delta n=0$. As an example, for a given quantum number $n\gtrsim 1$ which labels the wave function $\Psi_{n,j}$, there are eight energy levels j which couple to eight other energy levels j', associated with the wavefunction $\Psi_{n\pm 1,j'}$. The magnitude of the coupling between energy levels $E_{n,j}$ and $E_{n\pm 1,j'}$ is calculated from the (j,j') matrix element of Eqs. (55) and (57). Thus, all energy bands are, in principle, coupled, although the magnitude of the coupling varies greatly from one case to another. In particular, there is a weak coupling between bands of opposite spin, and the magnitude of these matrix elements depends explicitly on the off-diagonal spin-orbit matrix elements $\lambda_{1,3}$ and $\lambda_{2,3}$. In fact, one method of evaluating the band parameters $\lambda_{1,3}$ and $\lambda_{2,3}$ is a high-resolution magnetoreflection experiment in the limit of low photon energy and of high magnetic fields.

With or without spin-orbit interaction, harmonics connecting states $\Psi_{n,j}$ and $\Psi_{n\pm 2,j'}$ are expected, and the intensity of these weaker transitions is proportional to $\pi_{3,3}{}^2\propto\gamma_3{}^2$. Thus, a study of the relative intensity of the allowed transitions and harmonics in the magnetoreflection experiment could provide numerical values for the trigonal warping band parameter γ_3.

The general effective-mass Hamiltonian developed in this paper provides a framework for the detailed interpretation of the magnetoreflection and de Haas–van Alphen experiments, thereby yielding numerical values for the spin-orbit band parameters. Such an analysis is to be the subject of forthcoming publications.[3,15]

ACKNOWLEDGMENTS

The authors would like to express their appreciation for stimulating discussions with Professor J. W. McClure, Dr. J. G. Mavroides, and Dr. S. J. Williamson.

APPENDIX A. TIME-REVERSAL SYMMETRY

In addition to the spatial symmetry operations for the group of the wave vector given in Table I, there are two other symmetry operations which leave the graphite effective-mass Hamiltonian invariant. These operations are time-reversal and spatial-inversion-translation, denoted, respectively, by K and $\mathcal{J}=(J|\mathbf{t}_4/2)$. Here $\mathcal{J}$ represents the compound operation of spatial inversion J followed by a $\mathbf{t}_4/2$ translation. The need for invoking time-reversal symmetry when spin is included is implied by the additional degeneracy of the irreducible representations S_4 and S_5 for the double group. In fact, time-reversal symmetry requires a double degeneracy in the energy levels not only along the zone edge, but also at a general point in the Brillouin zone.

The effect of these operations on wave functions which transform as the irreducible representations of the group of the wave vector $G(S)$ can be studied by using as basis functions appropriate linear combinations of tight-binding functions. Following the notation of Slonczewski and Weiss,[1] these basis functions are written as

$$\Psi_{11}=(1/\sqrt{2})(a+a'), \quad (A1a)$$

$$\Psi_{21}=(1/\sqrt{2})(a-a'), \quad (A1b)$$

$$\Psi_{31}=b', \quad (A1c)$$

$$\Psi_{32}=b, \quad (A1d)$$

in which the tight binding functions associated with the A, A', B, and B' atomic sites are constructed from atomic $2p_z$ orbitals $\psi_z(\mathbf{r}-\mathbf{d})$ centered at $\mathbf{d}$ on a Bravais lattice having N lattice sites,

$$a(\mathbf{k}_s)=\frac{1}{\sqrt{N}}\sum_{\mathbf{d}} e^{i\mathbf{k}_s\cdot\mathbf{d}}\psi_z(\mathbf{r}-\mathbf{d}), \quad (A2a)$$

$$a'(\mathbf{k}_s)=\frac{1}{\sqrt{N}}\sum_{\mathbf{d}} e^{i\mathbf{k}_s\cdot(\mathbf{d}+\mathbf{t}_{A'})}\psi_z(\mathbf{r}-\mathbf{d}-\mathbf{t}_{A'}), \quad (A2b)$$

$$b(\mathbf{k}_s)=\frac{1}{\sqrt{N}}\sum_{\mathbf{d}} e^{i\mathbf{k}_s\cdot(\mathbf{d}+\mathbf{t}_B)}\psi_z(\mathbf{r}-\mathbf{d}-\mathbf{t}_B), \quad (A2c)$$

$$b'(\mathbf{k}_s)=\frac{1}{\sqrt{N}}\sum_{\mathbf{d}} e^{i\mathbf{k}_s\cdot(\mathbf{d}+\mathbf{t}_{B'})}\psi_z(\mathbf{r}-\mathbf{d}-\mathbf{t}_{B'}), \quad (A2d)$$

in which the vectors $\mathbf{k}_s$ and $\mathbf{t}_A$, $\mathbf{t}_{A'}$, $\mathbf{t}_B$, $\mathbf{t}_{B'}$ are defined in Eqs. (4) and (1), respectively. By direct calculation, the effect of the spatial-inversion-translation operation on the basis functions is found to be

$$\mathcal{J}\begin{bmatrix}\Psi_{11}(\mathbf{k}_s)\\ \Psi_{21}(\mathbf{k}_s)\\ \Psi_{31}(\mathbf{k}_s)\\ \Psi_{32}(\mathbf{k}_s)\end{bmatrix}=e^{i\mathbf{k}_s\cdot\mathbf{t}_4/2}\begin{bmatrix}-\Psi_{11}(-\mathbf{k}_s)\\ +\Psi_{21}(-\mathbf{k}_s)\\ -\Psi_{32}(-\mathbf{k}_s)\\ -\Psi_{31}(-\mathbf{k}_s)\end{bmatrix}, \quad (A3)$$

and it is readily seen that $\mathcal{J}$ is unitary, i.e., $\mathcal{J}^\dagger\mathcal{J}=1$. Whereas the spatial-inversion-translation operator acts only on the spatial wave functions, the time-reversal operator acts on both the spatial and spin wave functions[16]

$$K=i\sigma_y K_0, \quad (A4)$$

in which σ_y is the Pauli spin matrix and K_0 is the complex conjugation operator. The effect of K_0 on the basis

[15] S. J. Williamson, S. Foner, and M. S. Dresselhaus (to be published).

[16] C. Kittel, *Quantum Theory of Solids* (John Wiley & Sons, Inc., New York, 1963), p. 182.

functions is merely to replace $\mathbf{k}_s$ by $-\mathbf{k}_s$, since the atomic $2p_z$ functions $\psi_z(\mathbf{r}-\mathbf{d})$ can always be made real by taking appropriate linear combinations in the azimuthal quantum number. Using the definitions $\uparrow=\begin{pmatrix}1\\0\end{pmatrix}$ for the spin up state, and $\downarrow=\begin{pmatrix}0\\1\end{pmatrix}$ for the spin down state, the effect of the operator

$$i\sigma_y=\begin{pmatrix}0 & -1\\ 1 & 0\end{pmatrix} \tag{A5}$$

on the spin wave functions is

$$\begin{aligned} i\sigma_y\uparrow&=\downarrow,\\ i\sigma_y\downarrow&=-\uparrow. \end{aligned} \tag{A6}$$

Using the commutation relations for the $\mathcal{J}$ and K operators with linear and angular momenta,[16] these results for the time-reversal and spatial-inversion-translation operators can be applied to obtain additional restrictions on the matrix elements of the "$\mathbf{k}\cdot\mathbf{p}$" and spin-orbit Hamiltonians. For example, the "$\mathbf{k}\cdot\mathbf{p}$" matrix elements $\pi_{1,3}$ and $\pi_{2,3}$ can be shown to be real by the following argument:

$$\begin{aligned} \pi_{1,3}&=(\Psi_{11}(\mathbf{k}_s),p_-\Psi_{31}(\mathbf{k}_s))\\ &=(K_0p_-\Psi_{31}(\mathbf{k}_s),K_0\Psi_{11}(\mathbf{k}_s))\\ &=-(p_+\Psi_{31}(-\mathbf{k}_s),\Psi_{11}(-\mathbf{k}_s))\\ &=-(p_+\mathcal{J}\Psi_{32}(\mathbf{k}_s),\mathcal{J}\Psi_{11}(\mathbf{k}_s))\\ &=(\Psi_{32}(\mathbf{k}_s),p_-\Psi_{11}(\mathbf{k}_s))=\pi_{1,3}{}^* \end{aligned} \tag{A7}$$

in which the unitarity of $\mathcal{J}$ has been utilized. The reality of $\pi_{2,3}$ can be established by a similar argument.

Restrictions on the spin-orbit matrix elements can also be obtained. For example, the matrix element $\lambda_{1,2}{}^z$ is necessarily real, since

$$\begin{aligned} \lambda_{1,2}{}^z&=(\Psi_{11}(\mathbf{k}_s)\uparrow,L_z\sigma_z\Psi_{21}(\mathbf{k}_s)\uparrow)\\ &=(KL_z\sigma_z\Psi_{21}(\mathbf{k}_s)\uparrow,K\Psi_{11}(\mathbf{k}_s)\uparrow)\\ &=-(\mathcal{J}\Psi_{21}(\mathbf{k}_s)\downarrow,L_z\sigma_z\mathcal{J}\Psi_{11}(\mathbf{k}_s)\downarrow)\\ &=-(\Psi_{21}(\mathbf{k}_s)\downarrow,L_z\sigma_z\Psi_{11}(\mathbf{k}_s)\downarrow)=\lambda_{1,2}{}^z. \end{aligned} \tag{A8}$$

The matrix element $\lambda_{3,3}{}^z$ is necessarily real, since it is the diagonal matrix element of a Hermitian matrix. Thus, the two spin-orbit matrix elements which couple like spins are real. On the other hand, the spin-orbit matrix elements coupling unlike spins are purely imaginary. This result follows from the argument given in Eq. (A8) when applied to the matrix elements $\lambda_{1,3}$ and $\lambda_{2,3}$; i.e.,

$$\begin{aligned} \lambda_{1,3}&=(\Psi_{11}(\mathbf{k}_s)\uparrow,L_-\sigma_+\Psi_{31}(\mathbf{k}_s)\downarrow)\\ &=-(\Psi_{32}(\mathbf{k}_s)\uparrow,L_-\sigma_+\Psi_{11}(\mathbf{k}_s)\downarrow)=-\lambda_{1,3}{}^*\\ \lambda_{2,3}&=-(\Psi_{21}(\mathbf{k}_s)\uparrow,L_-\sigma_+\Psi_{31}(\mathbf{k}_s)\downarrow)\\ &=-(\Psi_{32}(\mathbf{k}_s)\uparrow,L_-\sigma_+\Psi_{21}(\mathbf{k}_s)\downarrow)=-\lambda_{2,3}{}^*. \end{aligned} \tag{A9}$$

The matrix element $\lambda_{3,3}$ couples unlike spin states between the two degenerate basis functions Ψ_{31} and Ψ_{32}. The time-reversal argument of Eq. (A8) yields

$$\begin{aligned} \lambda_{3,3}&=(\Psi_{31}(\mathbf{k}_s)\uparrow,L_-\sigma_+\Psi_{32}(\mathbf{k}_s)\downarrow)\\ &=-(\Psi_{31}(\mathbf{k}_s)\uparrow,L_-\sigma_+\Psi_{32}(\mathbf{k}_s)\downarrow)=-\lambda_{3,3}, \end{aligned} \tag{A10}$$

which requires that $\lambda_{3,3}$ vanish identically.

APPENDIX B. WAVE FUNCTIONS IN THE EXTENDED ZONE

The symmetry properties of the wave functions under translation in wave-vector space by $\mathbf{K}_4$ are established. Because of the necessary twofold degeneracy of the energy levels at point H, it is sometimes useful to consider a double zone, which is constructed from the first Brillouin zone by a $\mathbf{K}_4$ translation. An explicit derivation is given for the tight binding basis functions of Appendix A, but similar considerations apply to symmetrized plane wave basis functions. Since $\mathbf{K}_4\cdot\mathbf{d}=2\pi n$ for $n=0, \pm1, \pm2, \cdots$, a translation of the wave vector by $\mathbf{K}_4$ in the functions defined by Eq. (A2) yields

$$a(\mathbf{k}_s\pm\mathbf{K}_4)=a(\mathbf{k}_s), \tag{B1a}$$

$$a'(\mathbf{k}_s\pm\mathbf{K}_4)=-a'(\mathbf{k}_s), \tag{B1b}$$

$$b(\mathbf{k}_s\pm\mathbf{K}_4)=b(\mathbf{k}_s), \tag{B1c}$$

$$b'(\mathbf{k}_s\pm\mathbf{K}_4)=-b'(\mathbf{k}_s), \tag{B1d}$$

and the results of Eq. (16) follow immediately.